Persistent eNOS activation secondary to caveolin-1 deficiency induces pulmonary hypertension in mice and humans through PKG nitration

You-Yang Zhao,[1,2] Yidan D. Zhao,[1,2] Muhammad K. Mirza,[1,2] Julia H. Huang,[1,2] Hari-Hara S.K. Potula,[1,2] Steven M. Vogel,[1,2] Viktor Brovkovych,[1,2] Jason X.-J. Yuan,[3] John Wharton,[4] and Asrar B. Malik[1,2]

[1]Department of Pharmacology and [2]Center for Lung and Vascular Biology, University of Illinois College of Medicine, Chicago, Illinois, USA. [3]Department of Medicine, UCSD, La Jolla, California, USA. [4]Department of Experimental Medicine and Toxicology, Faculty of Medicine, Imperial College London, London, United Kingdom.

Pulmonary hypertension (PH) is an unremitting disease defined by a progressive increase in pulmonary vascular resistance leading to right-sided heart failure. Using mice with genetic deletions of caveolin 1 (*Cav1*) and eNOS (*Nos3*), we demonstrate here that chronic eNOS activation secondary to loss of caveolin-1 can lead to PH. Consistent with a role for eNOS in the pathogenesis of PH, the pulmonary vascular remodeling and PH phenotype of *Cav1*$^{-/-}$ mice were absent in *Cav1*$^{-/-}$*Nos3*$^{-/-}$ mice. Further, treatment of *Cav1*$^{-/-}$ mice with either MnTMPyP (a superoxide scavenger) or L-NAME (a NOS inhibitor) reversed their pulmonary vascular pathology and PH phenotype. Activation of eNOS in *Cav1*$^{-/-}$ lungs led to the impairment of PKG activity through tyrosine nitration. Moreover, the PH phenotype in *Cav1*$^{-/-}$ lungs could be rescued by overexpression of PKG-1. The clinical relevance of the data was indicated by the observation that lung tissue from patients with idiopathic pulmonary arterial hypertension demonstrated increased eNOS activation and PKG nitration and reduced caveolin-1 expression. Together, these data show that loss of caveolin-1 leads to hyperactive eNOS and subsequent tyrosine nitration–dependent impairment of PKG activity, which results in PH. Thus, targeting of PKG nitration represents a potential novel therapeutic strategy for the treatment of PH.

Introduction

Pulmonary hypertension (PH) is characterized by a progressive increase in pulmonary vascular resistance (PVR) and vascular remodeling, which without treatment leads to right-heart failure and death often within 2–3 years of diagnosis (1, 2). There are currently limited options available for the prevention and treatment of progressive PH (3, 4). Increased pulmonary vascular tone and severe structural remodeling of distal pulmonary arteries are the primary determinants of increased PVR. PH types with different etiologies share several common features: increasing severity of pulmonary vasoconstriction, remodeling of pulmonary microvessels, and intravascular thrombosis (1, 5, 6). These changes result in increased medial thickness, microvascular occlusion, and formation of plexiform lesions, all of which contribute to the mechanism of PH (1, 5, 6). Studies have described mutations of bone morphogenetic protein receptor type II in patients with PH (7, 8). As only 10%–15% of these individuals go on to develop the severe form of the disease (8, 9), it is likely that other genetic and environmental factors are also important (10). One such factor may be the dysfunction or injury of pulmonary vascular endothelial cells resulting in aberrant production of endothelium-derived mediators such as endothelin-1 and NO (2, 11), which may have a role in the pathogenesis of PH.

NO is a vasodilator regulating multiple physiological and pathophysiological processes, including host-defense response, neuronal communication, and vascular tone (12). High-output NO production by iNOS is considered detrimental in vascular disorders, whereas low-output eNOS-derived NO in general is regarded as protective (13). The eNOS isoform, predominantly expressed in endothelial cells, regulates basal pulmonary and peripheral vasomotor tone (14). eNOS activity is controlled by fatty acid modification, phosphorylation, and interaction with effector molecules such as caveolin-1 and heat shock protein 90 (hsp90) (15). Binding of caveolin-1 to eNOS has been shown to be a crucial negative regulator of eNOS activity (16, 17). Caveolin-1 also regulates signal transduction by concentrating multiple signaling molecules at its scaffold microdomain (18). Studies have identified an important pathogenic role of caveolin-1 in the development of PH in animal models (19–22). *Cav1*$^{-/-}$ mice developed PH and right-ventricular hypertrophy in association with pulmonary vascular remodeling, hypercellularity, and alveolar septal thickening (19–21). Caveolin-1 deficiency was also seen in rat models of PH (22, 23), and the cell-permeable Cav1 inhibitory peptide prevented the development of monocrotaline-induced

Authorship note: Yidan D. Zhao and Muhammad K. Mirza contributed equally to this work.

Conflict of interest: The authors have declared that no conflict of interest exists.

Nonstandard abbreviations used: hsp90, heat shock protein 90; IPAH, idiopathic pulmonary arterial hypertension; L-NAME, *N*-nitro-L-arginine methyl ester; MnTMPyP, manganese (III) tetrakis (1-methyl-4-pyridyl) porphyrin pentachloride; NO_x, nitrate/nitrite; PH, pulmonary hypertension; PVR, pulmonary vascular resistance; RVSP, right-ventricular systolic pressure; sGC, soluble guanylyl cyclase; SIN-1, 3-morpholinosydnonimine; VASP, vasodilator-stimulated phosphoprotein.

Citation for this article: *J. Clin. Invest.* **119**:2009–2018 (2009). doi:10.1172/JCI33338.

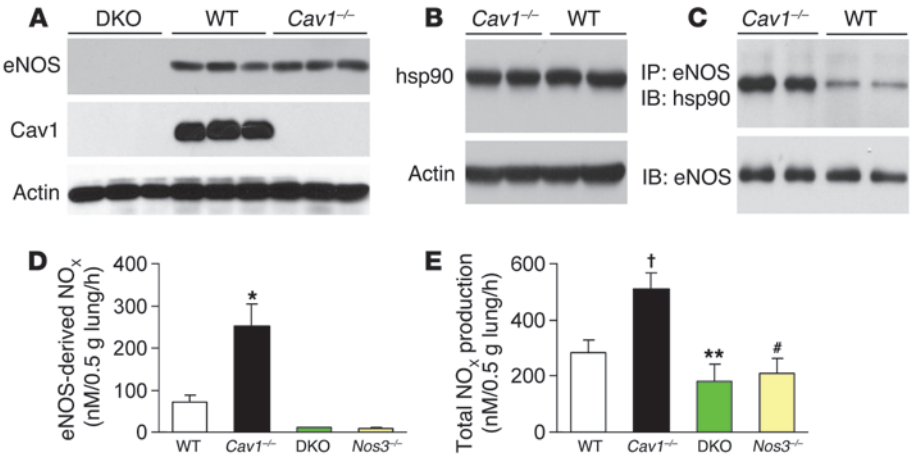

Figure 1
Chronic eNOS activation in *Cav1*$^{-/-}$ lungs. (**A**) Western blot analysis of caveolin-1 and eNOS expression in lungs from 2-month-old mice. Lung lysate (20 μg per lane) was loaded and immunoblotted with antibodies against mouse eNOS, caveolin-1, and β-actin (loading control). Neither caveolin-1 nor eNOS was detected in DKO lungs. (**B**) Similar protein expression of hsp90 in *Cav1*$^{-/-}$ and WT lungs. (**C**) Increased eNOS-hsp90 association in *Cav1*$^{-/-}$ lungs. Lung lysates (500 μg) were immunoprecipitated with anti-eNOS and immunoblotted with anti-hsp90. The same blot was immunoblotted with anti-eNOS. (**D**) Quantitative analysis of eNOS-derived NO_x in mouse lungs. eNOS-derived NO_x was determined using the Griess reagent in the presence of iNOS and nNOS inhibitors but without addition of the eNOS agonist, e.g., calcium ionophore A23187. Data are shown as mean ± SD (n = 4–5). *P < 0.001 versus WT (n = 4–6). *Cav1*$^{-/-}$ lungs produced 3.5-fold more eNOS-derived NO_x than WT lungs. (**E**) Total NO_x production in mouse lungs. Total NO_x production was determined with the Griess reagent. Data are expressed as mean ± SD (n = 4–5). †P < 0.05, *Cav1*$^{-/-}$ versus WT; **P < 0.01, DKO versus WT; #P < 0.05, *Nos3*$^{-/-}$ versus WT.

PH (24). In addition, decreased expression of caveolin-1, predominantly in endothelial cells, was observed in lungs of patients with severe idiopathic pulmonary arterial hypertension (IPAH) (23, 25). In the present study, we addressed the potentially important mechanism of pulmonary vascular remodeling and PH associated with caveolin-1 deficiency. We determined the role of eNOS-derived NO in the pathogenesis of PH using double-knockout mice deficient in *Cav1* and eNOS (*Nos3*) (DKO mice). Our studies showed that persistent eNOS activation secondary to caveolin-1 deficiency induced the nitration of PKG and the resultant impairment of its kinase activity. We demonstrated that this post-translational modification in a mouse model and in lungs of patients with IPAH is a critical determinant of the pathogenesis of PH.

Results

Genetic deletion of Nos3 in Cav1$^{-/-}$ *mice prevents PH. Nos3*$^{-/-}$ mice were bred into the background of *Cav1*$^{-/-}$ mice to generate mice with deletions of both *Cav1* and *Nos3*. DKO mice were indistinguishable from WT littermates. We observed that 85% (n = 200) of the DKO mice survived at least 18 months, the same as the life expectancy of WT mice. To eliminate any background effects from either the *Nos3*$^{-/-}$ or *Cav1*$^{-/-}$ line on the observed phenotype, F_4 or higher generations were used in the present studies. As shown in Figure 1, *Cav1*$^{-/-}$ and WT lungs expressed a similar amount of eNOS and its chaperone protein hsp90. However, eNOS association with hsp90 was drastically increased in *Cav1*$^{-/-}$ compared with WT lungs (Figure 1C). Basal eNOS-derived NO production as measured by nitrate

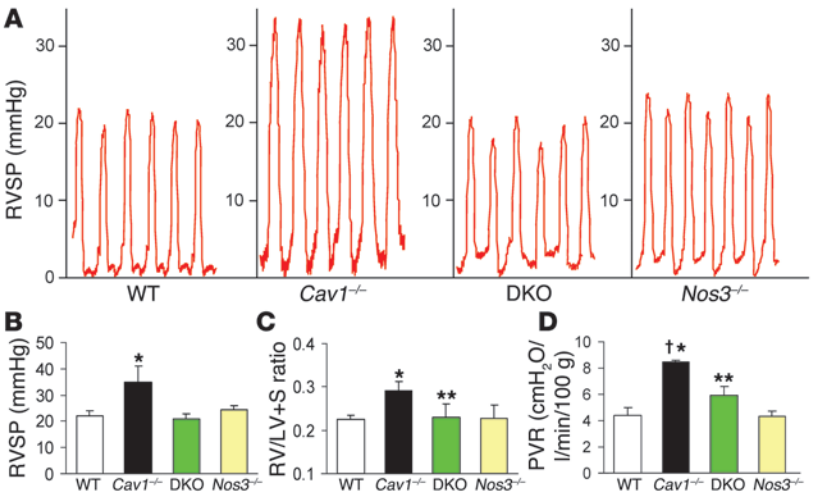

Figure 2
PH and increased PVR in *Cav1*$^{-/-}$ mice were prevented in DKO mice. (**A**) Representative RVSP tracings (each represents 1 second). (**B**) Normalized RVSP in DKO mice. RVSP was measured in age- and sex-matched 9-month-old mice. Data are expressed as mean ± SD. *P < 0.01, *Cav1*$^{-/-}$ versus WT or DKO (n = 6–8). (**C**) Restored RV/LV+S weight ratios in DKO mice. Right and left ventricles including septum (S) were dissected free of connective tissues from age- and sex-matched mice and weighed. Data are expressed as mean ± SD. *P < 0.01, *Cav1*$^{-/-}$ versus WT (n = 5–7); **P < 0.01, DKO versus *Cav1*$^{-/-}$ (n = 6–8). (**D**) Restored PVR in DKO lungs. Data are expressed as mean ± SD. *P < 0.01, *Cav1*$^{-/-}$ versus WT; †P < 0.05, *Cav1*$^{-/-}$ versus DKO; **P > 0.5, DKO versus WT (n = 4–6).

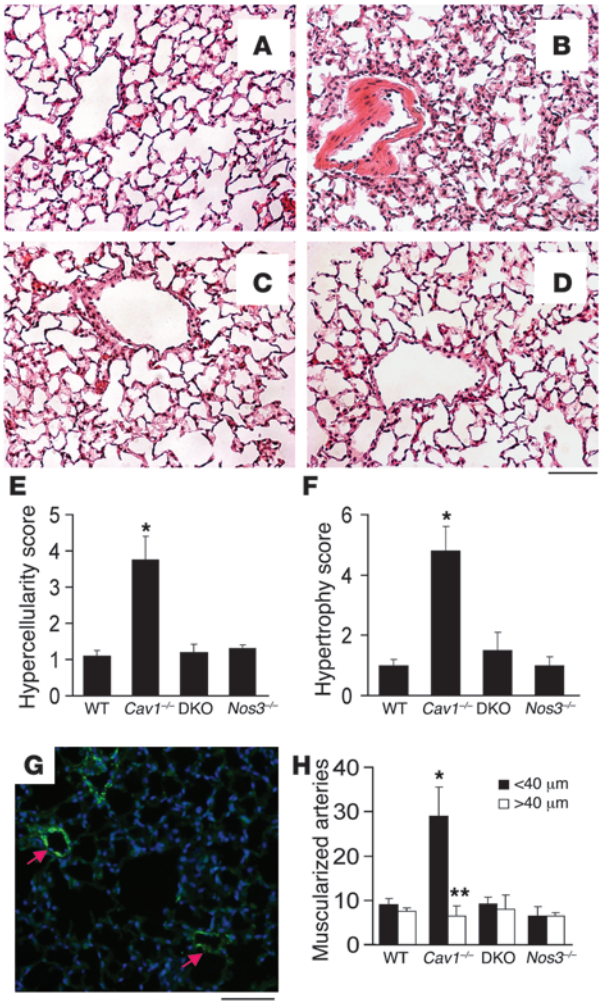

Figure 3
Prevention of pulmonary vascular remodeling induced by *Cav1* deletion in DKO mice. (**A**–**D**) Representative micrographs of H&E-stained lung sections from age- and sex-matched WT (**A**), *Cav1*$^{-/-}$ (**B**), DKO (**C**), and *Nos3*$^{-/-}$ (**D**) mice. Hypercellularity and medial thickening seen in *Cav1*$^{-/-}$ lungs were prevented in DKO lungs. Scale bar: 60 μm. (**E**) Histology grade score of hypercellularity in lung sections. Cellular hyperplasia was scored from 1 to 5, with 5 as the highest. Data are expressed as mean ± SD. *P < 0.01, *Cav1*$^{-/-}$ versus WT, DKO, or eNOS (n = 4–6). (**F**) Histology grade score of lung vascular hypertrophy. Medial thickness was scored from 1 to 6, with 6 being the highest. Data are expressed as mean ± SD. *P < 0.01 versus WT, DKO, or eNOS (n = 4–6). (**G**) Representative micrograph of immunostaining of *Cav1*$^{-/-}$ lung sections with anti–α-SMA (green). Arrows show muscularized distal pulmonary arterial vessels. Scale bar: 50 μm. (**H**). Quantification of muscularized pulmonary arterial vessels in mouse lung sections. α-SMA–positive vessels were counted in 20 fields (×200) of each lung section. Data are expressed as mean ± SD. *P < 0.01, *Cav1*$^{-/-}$ versus WT, DKO, or eNOS (n = 4–6); **P > 0.5, *Cav1*$^{-/-}$ versus WT, DKO, or eNOS. <40 μm, vessels with diameter less than 40 μm; >40 μm, vessels with diameter greater than 40 μm.

and nitrite (NO_x) production was 3.5-fold greater in *Cav1*$^{-/-}$ than WT lungs (Figure 1D), consistent with the activation of eNOS secondary to loss of caveolin-1 inhibition in vivo. There was little eNOS-derived NO_x produced in either *Nos3*$^{-/-}$ lungs or DKO lungs (Figure 1D). Similar expression of iNOS and nNOS was detected in lungs from WT, *Cav1*$^{-/-}$, and DKO mice, and the amount of iNOS-derived NO_x in *Cav1*$^{-/-}$ lungs was also similar to that in WT lungs (Supplemental Figure 1; supplemental material available online with this article; doi:10.1172/JCI33338DS1). Total NO_x production in *Cav1*$^{-/-}$ lungs was 1.8-fold greater than in WT (Figure 1E).

To determine the consequences of chronic activation of eNOS in *Cav1*$^{-/-}$ lungs, we measured right-ventricular systolic pressure (RVSP) (to reflect the pulmonary artery systolic pressure). *Cav1*$^{-/-}$ mice had significantly increased RVSP compared with WT mice (Figure 2, A and B). However, RVSP in DKO mice was the same as in WT. The weight ratio of right/left ventricle plus septum (RV/LV+S) was normal in DKO mice, in contrast to *Cav1*$^{-/-}$ mice, in which the ratio was increased (Figure 2C). PVR in DKO mice was reduced to the WT level (Figure 2D), indicating that PH occurring secondarily to increased PVR in *Cav1*$^{-/-}$ mice was the result of chronic eNOS activation.

Rescue of pulmonary vascular pathology in DKO mice. Studies have demonstrated severe lung hypercellularity and thickening of alveolar septa in *Cav1*$^{-/-}$ mice (19–21); thus, we addressed the possibility that chronically active eNOS in *Cav1*$^{-/-}$ mice was responsible for the lung pathology in these mice. DKO lungs exhibited normal alveolar-capillary structure and vessel wall thickness (Figure 3C) in contrast to *Cav1*$^{-/-}$ lungs (Figure 3B). Histological scoring showed normal pulmonary morphology in DKO lungs (Figure 3, E and F). To quantify the number of muscularized distal pulmonary arteries, an underlying feature of pulmonary vascular remodeling in PH, we stained lung sections with anti–α-SMA. *Cav1*$^{-/-}$ lungs exhibited a 3-fold increase in muscularized distal arteries (<40 μm in diameter) compared with WT, whereas a similar number of muscularized large vessels was seen in *Cav1*$^{-/-}$ and WT lungs (Figure 3, G and H). The number of muscularized distal and large vessels in DKO lungs was similar to that in the WT and *Nos3*$^{-/-}$ lungs (Figure 3H).

To address the molecular basis of the hyperplasia and pulmonary vascular remodeling seen in *Cav1*$^{-/-}$ lungs, we examined ERK signaling and expression of genes regulating cell-cycle progression. As shown in Figure 4A, ERK signaling was increased in *Cav1*$^{-/-}$ lungs compared with either WT or DKO. Quantitative RT-PCR analysis showed that the mRNA level of $p21^{Cip1}$, a cyclin-dependent kinase inhibitor, was decreased 5-fold in *Cav1*$^{-/-}$ lungs compared with WT, whereas $p21^{Cip1}$ expression in DKO lungs was restored (Figure 4B). Interestingly, expression of the growth factors IGF-I and VEGF-A was increased in *Cav1*$^{-/-}$ lungs, whereas they were normal in DKO lungs (Figure 4, C and D). Thus, activation of ERK signaling and downregulation of $p21^{Cip1}$ in *Cav1*$^{-/-}$ lungs may be the result of increased expression of these growth factors in *Cav1*$^{-/-}$ lungs.

Tyrosine nitration of PKG secondary to caveolin-1 deficiency impairs PKG activity. NO reacts with superoxide to form the damaging reactive nitrogen species peroxynitrite, which modifies proteins and may interfere with their function through tyrosine nitration (26–28). Immunostaining of nitrotyrosine, a surrogate measure of peroxynitrite, showed that *Cav1*$^{-/-}$ lungs had greater nitrotyrosine expression than WT and DKO lungs (Figure 5A), indicating the formation of peroxynitrite in *Cav1*$^{-/-}$ lungs. Prominent nitrotyrosine immunostaining was also evident in *Cav1*$^{-/-}$ pulmonary vasculature, including muscularized distal arteries (Figure 5A). Western blotting also demonstrated increased tyrosine nitration of proteins in *Cav1*$^{-/-}$ lungs (Figure 5B), whereas no difference in *S*-nitrosylation of proteins was seen in *Cav1*$^{-/-}$ and WT lungs (Figure 5C).

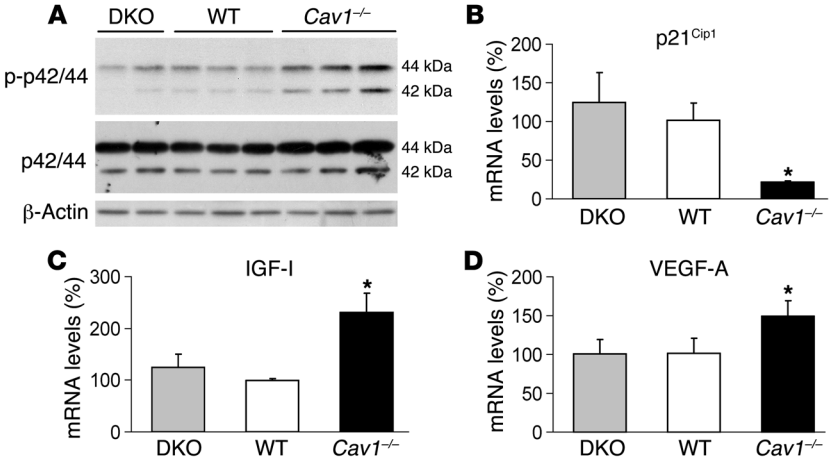

Figure 4

Normalized ERK signaling and gene expression in DKO lungs. (**A**) Western blot analysis of ERK signaling. Phosphorylation of p42/44 MAPK was detected with anti–phospho-p42/44 in lung lysates (30 μg per lane). The same blot was immunoblotted with anti-p42/44 for detection of total p42/44 and with anti–β-actin for loading control. (**B**–**D**) Quantitative analysis of gene expression in mouse lungs. Total RNA was isolated from lungs collected from 2-month-old mice, and mRNA levels of $p21^{Cip1}$ (**B**), IGF-I (**C**), and VEGF-A (**D**) were analyzed with quantitative SYBR Green RT-PCR assay. mRNA levels of cyclophilin were used for normalization. Data are expressed as mean ± SD (n = 3–5). *$P < 0.01$ versus WT or DKO. Expression of $p21^{Cip1}$ and growth factors IGF-I and VEGF-A was normalized in DKO lungs (similar to that in WT lungs).

We determined the activities of soluble guanylyl cyclase (sGC) and PKG, the two major downstream targets of NO signaling (29), to investigate whether their functions were impaired by tyrosine nitration in *Cav1*$^{-/-}$ lungs. Baseline sGC activity and maximal activity after stimulation with sodium nitroprusside, a NO donor, were similar in WT, *Cav1*$^{-/-}$, and DKO lungs (Supplemental Figure 2). In sharp contrast, basal PKG activity in *Cav1*$^{-/-}$ lungs was 30% less than that in the WT group (Figure 6A) and also following the addition of 2.5 μM cGMP (Figure 6B). PKG activities in DKO lungs were restored to levels similar to those in WT lungs (Figure 6, A and B). PKG dysfunction in *Cav1*$^{-/-}$ lungs could not be ascribed to reduced cGMP production, since *Cav1*$^{-/-}$ lungs in fact exhibited higher cGMP concentrations (Supplemental Figure 2). The protein levels of PKG-1 were also similar in WT, *Cav1*$^{-/-}$, and DKO lungs (Figure 6C). Quantitative RT-PCR demonstrated similar mRNA expression of PKG-1 and PKG-2 in mouse lungs (Supplemental Figure 3). These data suggest that impaired PKG activity in *Cav1*$^{-/-}$ lungs is the result of post-translation modification. Indeed, we observed markedly increased nitrotyrosine modification of PKG-1 in *Cav1*$^{-/-}$ lungs as compared with DKO and WT lungs (Figure 6C). In contrast, *S*-nitrosylation of PKG-1 in *Cav1*$^{-/-}$ lungs was minimal and similar to that in WT and DKO lungs (Supplemental Figure 4).

To address the role of peroxynitrite in the mechanism of the observed impairment of PKG activity, we treated human pulmonary artery smooth muscle cells with 3-morpholinosydnonimine (SIN-1), a superoxide and NO donor that forms peroxynitrite simultaneously (30). SIN-1 concentrations as low as 10 μM were shown to cause marked PKG tyrosine nitration (Figure 6D) and decreased PKG activity (Figure 6, E and F). Furthermore, in vitro treatment of purified PKG-1 with peroxynitrite resulted in decreased PKG activity in a concentration-dependent manner, whereas DETA NONOate, a NO donor, even at 100 μM failed to suppress PKG activity (Figure 7A).

To identify the target tyrosine residues responsible for impairment of PKG activity upon nitration, we mutated all tyrosine residues in the catalytic domain of human PKG-1α into phenylalanine and expressed these myc-tagged PKG-1 mutants with either single or double mutations in human lung microvascular endothelial cells. As shown in Figure 7, B and C, mutation of either Tyr345 or Tyr549 resulted in no impairment of PKG activity following peroxynitrite treatment in contrast to other mutations and WT PKG-1. Accordingly, these PKG-1 mutants exhibited diminished tyrosine nitration in contrast to WT PKG-1 following peroxynitrite treatment (Figure 7D). Both Tyr345 and Tyr549 are conserved from zebrafish to human PKG-1 (Supplemental Figure 5). These data demonstrate that peroxynitrite formation impairs PKG activity through nitration at Tyr345 and Tyr549. Decreased kinase activity of PKG-1α mutant with mutation at Tyr524 was likely due to its location next to the activation loop (Figure 7B and Supplemental Figure 5).

Nitrative stress–mediated PKG dysfunction induces PH in Cav1$^{-/-}$ *mice*. To determine whether tyrosine nitration–mediated impairment of PKG activity was responsible for the development of PH in *Cav1*$^{-/-}$ mice, we carried out a series of experiments that included blocking peroxynitrite formation and overexpressing PKG. We first determined whether scavenging superoxide by manganese (III) tetrakis (1-methyl-4-pyridyl) porphyrin pentachloride (MnTMPyP, a superoxide dismutase mimetic) (31) could reverse PH in *Cav1*$^{-/-}$ mice. In this experiment, 8-month-old *Cav1*$^{-/-}$ mice received either saline or MnTMPyP (5 mg/kg, i.p. daily) for 6 weeks. We observed that MnTMPyP treatment reduced RVSP (Figure 8A). We also treated 8-month-old *Cav1*$^{-/-}$ mice with either *N*-nitro-L-arginine methyl ester (L-NAME, a NOS inhibitor) or its inactive analog D-NAME in drinking water (1 mg/ml) for 5 weeks. Inhibition of NO production by L-NAME treatment also reduced RVSP and the number of muscularized distal pulmonary arteries, whereas D-NAME had no effect (Figure 8B and Supplemental Figure 6). These data suggest that high levels of NO per se in *Cav1*$^{-/-}$ mice do not cause PH but that superoxide production is also important for its development; i.e., formation of peroxynitrite and resultant protein nitration are required for the development of PH.

We further tested the hypothesis that nitrative stress–induced PH in *Cav1*$^{-/-}$ mice is mediated by impaired PKG activity. Recombinant adenoviruses overexpressing human PKG-1 or LacZ were administered into lungs of 10-month-old WT and *Cav1*$^{-/-}$ mice via an intratracheal microspray device. At 7 days after infection, PKG-1 protein expression was elevated by 50% in AdvPKG-treated *Cav1*$^{-/-}$ lungs compared with AdvLacZ-treated control lungs (Figure 8C). PKG activity in AdvPKG-treated *Cav1*$^{-/-}$ lungs was restored to a level similar to that in WT lungs (Figure 8D). PKG-mediated phosphorylation of its substrate vasodilator-stimulated phosphoprotein (VASP) at residue Ser239 was also normalized in AdvPKG-treated *Cav1*$^{-/-}$ lungs (Supplemental Figure 7). Accordingly, we

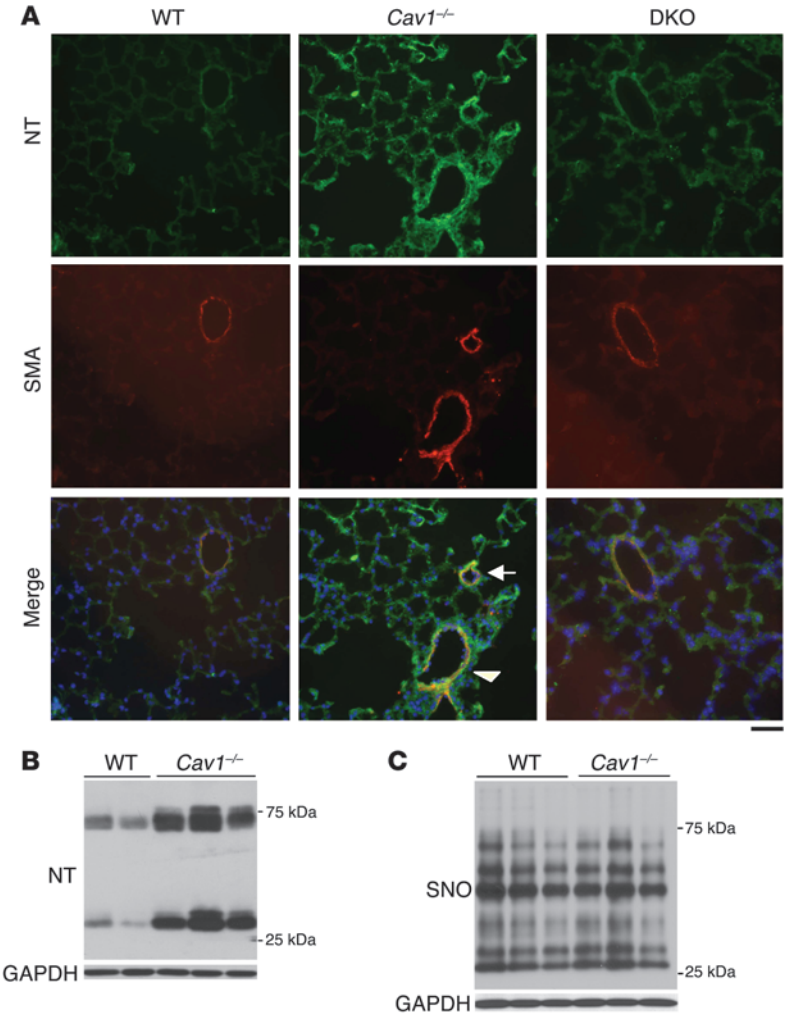

Figure 5
Increased tyrosine nitration of proteins in *Cav1*$^{-/-}$ mouse lungs. (**A**) Representative micrographs of immunostaining of lung sections with anti-nitrotyrosine (NT, green) and anti–α-SMA (SMA, red). Nuclei were counterstained with DAPI (blue). Nitrotyrosine was prominent in *Cav1*$^{-/-}$ lungs, including large artery (arrowhead) and muscularized distal artery (arrow). Scale bar: 40 μm. (**B**) Increased protein nitration in *Cav1*$^{-/-}$ mouse lungs. Forty micrograms of lung lysates was loaded per lane. Nitrated proteins were directly detected with anti-nitrotyrosine antibody. The same blot was blotted with anti-GAPDH for loading control. We observed primarily 2 groups of proteins at molecular weights of approximately 30 and 70 kDa, respectively, with markedly increased tyrosine nitration in *Cav1*$^{-/-}$ lungs. (**C**) *S*-nitrosylation of proteins in *Cav1*$^{-/-}$ and WT lungs was not different. *S*-nitrosylation (SNO) in biotin-labeled lung lysates (10 μg per lane) was directly detected by Western blotting with avidin-coupled reagents.

observed that restoration of PKG-1 activity in *Cav1*$^{-/-}$ lungs resulted in a significant decrease in RVSP and PVR, whereas minimal changes were seen in WT mice (Figure 8, E and F).

Increased eNOS activity and PKG tyrosine nitration in lungs of IPAH patients. To address the relevance of these observations in mice to the pathogenesis of IPAH in patients, we determined eNOS activity, PKG tyrosine nitration, and expression of caveolin-1, eNOS, and PKG-1 in lung tissues from IPAH patients. eNOS activities were increased in IPAH lungs compared with normal lungs (Figure 9A and Supplemental Figure 8), whereas eNOS expression was similar to that in normal lungs (Figure 9B). Caveolin-1 expression was decreased in IPAH lungs compared with normal lungs (Figure 9B), consistent with previous reports (23, 25). Moreover, tyrosine nitration of PKG-1 was markedly increased in IPAH lungs (Figure 9, B and C). We also observed that PKG-1 expression was increased 30% in IPAH lungs (Figure 9B; IPAH, 1.3 ± 0.3 versus normal, 1.0 ± 0.07; $P = 0.12$), suggesting a compensatory PKG protein expression in the face of the decreased PKG activity.

Discussion

We show here that chronic eNOS-derived NO production secondary to the loss of caveolin-1 inhibition is a critical factor in the mechanism of PH. We have demonstrated that increased production of eNOS-derived NO resulted in the impairment of PKG kinase activity through its tyrosine nitration. The essential observations in mice were recapitulated in lung tissue from IPAH patients. The pulmonary vascular changes seen in *Cav1*$^{-/-}$ lungs were prevented in the *Cav1*$^{-/-}$*Nos3*$^{-/-}$ DKO mice, and PH was reversed following treatment of *Cav1*$^{-/-}$ mice with either superoxide scavenger or NOS inhibitor and by adenovirus-mediated restoration of PKG activity in *Cav1*$^{-/-}$ lungs. We also identified Tyr345 and Tyr549 in the catalytic domain of human PKG-1α as responsible for the impairment of PKG activity upon nitration. Thus, the results demonstrate what we believe to be a novel mechanism of PH mediated by the impairment of PKG activity secondary to the tyrosine nitration of the kinase.

Caveolin-1, the scaffolding protein of caveolae, serves a key regulatory signaling function in endothelial cells (32). We observed that eNOS-derived NO_x production in the *Cav1*$^{-/-}$ lungs increased 3.5-fold compared with that in WT lungs, whereas eNOS protein expression was similar in the two groups. The activity of other NOS isoforms, iNOS and nNOS, did not differ in WT, *Cav1*$^{-/-}$, and DKO lungs. These data show a fundamental in vivo role of caveolin-1 as a negative regulator of eNOS activity (15–17). eNOS binds with caveolin-1 in the caveolar membrane such that upon agonist activation, hsp90 binds with the eNOS dissociated from caveolin-1

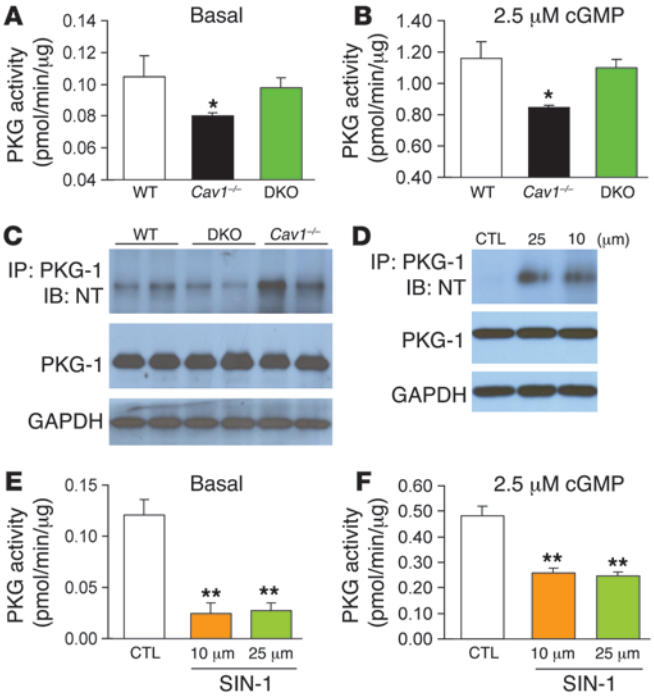

Figure 6
Impaired PKG kinase activity secondary to tyrosine nitration in *Cav1*$^{-/-}$ lungs. (**A** and **B**) In vitro PKG activity in lung lysates during the basal state (**A**) and following addition of 2.5 μM cGMP (**B**). Data are expressed as mean ± SD (n = 3–5). *P < 0.05, *Cav1*$^{-/-}$ versus WT or DKO. (**C**) Prominent tyrosine nitration of PKG detected in lung lysates from *Cav1*$^{-/-}$ mice. Lung lysates (150 μg) from WT, DKO, and *Cav1*$^{-/-}$ mice were immunoprecipitated with 2 μg anti–PKG-1 antibody overnight, and PKG tyrosine nitration was detected with anti-nitrotyrosine by Western blotting. Protein expression of PKG-1 in lung lysates was also determined directly by Western blotting with anti–PKG-1 antibody. The same blot was reprobed with an antibody against mouse GAPDH as a loading control. (**D**) PKG-1 tyrosine nitration in cultured human pulmonary artery smooth muscle cells following SIN-1 treatment. Subconfluent primary cultures were treated with SIN-1 at the indicated concentrations for 30 minutes, and each cell lysate (50 μg) was then used for immunoprecipitation and immunoblotting for detection of PKG-1 nitration. Each lysate (15 μg) was also used for direct immunoblotting with anti–PKG-1 and anti-GAPDH. CTL, control. (**E** and **F**) SIN-1 treatment resulted in a significant decrease in PKG activity in the basal state (**E**) and following addition of 2.5 μM cGMP (**F**). Data are shown as mean ± SD (n = 3). **P < 0.001 versus CTL.

and thereby promotes eNOS activation (33, 34). We demonstrated an increase in eNOS-hsp90 interaction in *Cav1*$^{-/-}$ lungs consistent with this model. Decreased eNOS-hsp90 interaction has been suggested to play a role in the pathogenesis of hypoxia-induced PH on the basis of decreased eNOS activity and NO bioavailability (35, 36). However, our data in *Cav1*$^{-/-}$ lungs showed that increased eNOS-hsp90 interaction was involved in the mechanism of PH due to persistent activation of eNOS and resultant increased formation of peroxynitrite.

eNOS-derived NO is usually considered to be protective (13). That is, low-output NO produced by eNOS induces vasodilatation and inhibits platelet aggregation, suppresses adhesion of neutrophils and monocytes to endothelial cells, and modulates vascular smooth cell proliferation and migration. In the present study, however, on the basis of genetic evidence from the DKO mice, we show a clear pathogenic role for the persistent production of eNOS-derived NO secondary to caveolin-1 deficiency in the development of PH.

In previous studies, increased production of NO in eNOS transgenic mice prevented the increase in RVSP, lung vascular remodeling, and right-ventricular hypertrophy induced by chronic hypoxia (37), and cell-based eNOS gene transfer also inhibited the development of PH induced by monocrotaline treatment in rats (38). We found in *Cav1*$^{-/-}$ mice, contrary to these observations, that increased eNOS activity was required for the development of PH. Genetic deletion of eNOS prevented the PH in *Cav1*$^{-/-}$ mice, while pharmacological inhibition of NO production by L-NAME reversed the PH in adult *Cav1*$^{-/-}$ mice. We observed that inhibition of superoxide production by the superoxide scavenger MnTMPyP also reversed the PH in adult *Cav1*$^{-/-}$ mice. Thus, a high concentration of NO itself in *Cav1*$^{-/-}$ mice did not cause PH, but NO coupled to superoxide production is critically important for the development of PH. The caveolin-1 deficiency–induced production of superoxide and eNOS-derived NO reacted to form peroxynitrite and induced PH in *Cav1*$^{-/-}$ lungs. Studies have shown that NO alone was incapable of inducing tissue injury even at high concentrations (39), whereas NO in the presence of superoxide produced peroxynitrite, thereby causing severe nitrative stress and tissue injury (26–28), findings consistent with our observations. Taken together, our data show the fundamental role of caveolin-1 in the pathogenesis of PH such that disruption of the negative regulation of eNOS by caveolin-1 leads to pulmonary vascular remodeling and PH.

Studies have suggested that eNOS uncoupling may be sufficient to increase the production of superoxide in *Cav1*$^{-/-}$ lungs and may thus mediate PH (40). Treatment of neonatal *Cav1*$^{-/-}$ mice with tetrahydrobiopterin, an essential cofactor for all 3 NOS isoforms (41, 42), prevented PH (40). However, in other studies, eNOS uncoupling alone did not cause PH (37). eNOS transgenic mice failed to develop PH but were resistant to hypoxia-induced PH (37), even though these mice exhibited eNOS uncoupling (43). L-NAME inhibition of NOS in neonatal *Cav1*$^{-/-}$ mice (44) and restoration of caveolin-1 expression in endothelial cells of *Cav1*$^{-/-}$ mice (45) prevented PH in *Cav1*$^{-/-}$ mice. Since none of these studies directly examined eNOS activation, they provide circumstantial evidence concerning the role of eNOS activation secondary to caveolin-1 deficiency in the pathogenesis of PH. It is well known that tetrahydrobiopterin activates all 3 isoforms of NOS (41, 42), whereas L-NAME inhibits all isoforms. Studies in a different ex vivo mouse lung model show that inhibition of NO production by L-NAME paradoxically increased PVR, with the effect being more pronounced in *Cav1*$^{-/-}$ compared with WT lungs (46). These results may be ascribed to differences inherent in the ex vivo lung model compared with the intact animal. Our studies using *Cav1*$^{-/-}$*Nos3*$^{-/-}$ DKO mice have demonstrated the essential role of eNOS-derived NO production and peroxynitrite formation in the mechanism of PH in *Cav1*$^{-/-}$ mice.

NO mediates vasodilatation through the activation of the sGC/cGMP/PKG signaling pathway (29). We observed that PKG activity was impaired in *Cav1*$^{-/-}$ lungs even in the face of high NO concen-

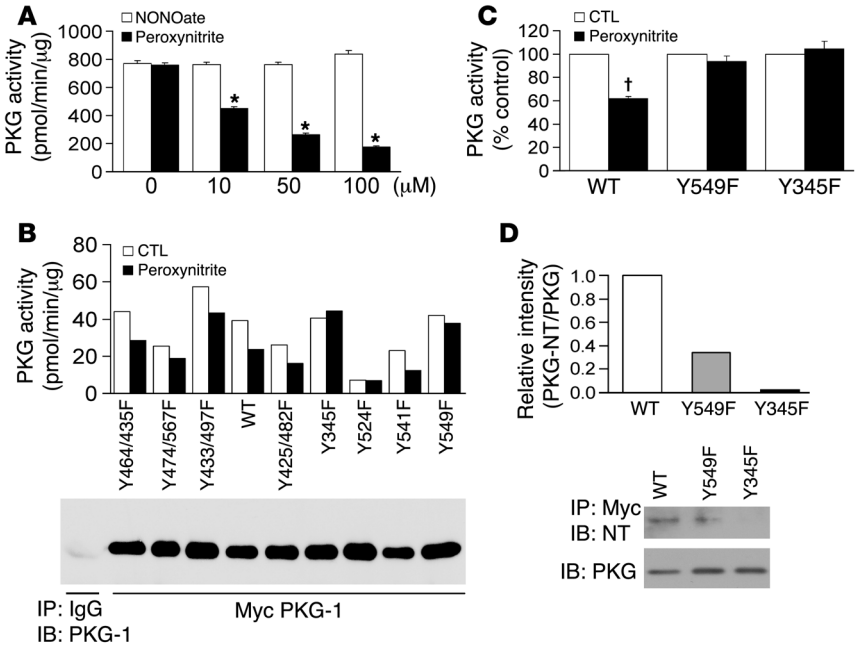

Figure 7

Identification of target tyrosine residues responsible for the impairment of PKG kinase activity upon nitration. (**A**) Dose-dependent impairment of PKG activity by peroxynitrite. Purified PKG-1 was incubated with peroxynitrite at the indicated concentrations for 14 minutes at room temperature or with DETA NONOate (NONOate) for 30 minutes in the dark at room temperature. Kinase activity was then assayed. Data are expressed mean ± SD (n = 3). *P < 0.05 versus control (0 μM). (**B**) Screening of PKG-1α mutants with in vitro kinase assay. At 48 hours after transfection, myc-tagged WT and PKG-1α mutants were immunoprecipitated with anti-myc beads and aliquoted for incubation with either peroxynitrite (100 μM) or the same amount of 0.1N NaOH only (CTL). In vitro kinase assay was then performed to determine PKG activity. PKG activity is expressed as picomoles/minute/microgram cell lysates. Western blotting was used to detect the protein levels of PKG-1α. (**C**) Validation of target tyrosine residues. At 48 hours after transfection, myc-tagged WT and PKG-1α mutants were immunoprecipitated for tyrosine nitration and in vitro kinase assay. Kinase activity following peroxynitrite incubation was normalized to that of the respective control. Data are expressed as mean ± SD (n = 3). †P < 0.05 versus either PKG-1α mutant. (**D**) Diminished tyrosine nitration of PKG-1 mutants. After 14 minutes incubation with peroxynitrite (250 μM) at room temperature, the anti-myc immunoprecipitates were used for Western blotting to detect tyrosine nitration. The intensity of each band of PKG-1 tyrosine nitration was normalized to the intensity of the respective PKG-1 band (PKG-NT/PKG).

trations, whereas sGC activity was not affected. There was markedly increased peroxynitrite production in *Cav1*$^{-/-}$ lungs, as evidenced by the increased nitrotyrosine immunostaining and protein tyrosine nitration. In contrast, DKO and WT lungs produced little peroxynitrite. It is known that peroxynitrite affects protein function through tyrosine nitration (26–28). We observed that PKG was in fact tyrosine-nitrated in *Cav1*$^{-/-}$ lungs. Decreased PKG activity was probably the result of PKG tyrosine nitration, since PKG expression in *Cav1*$^{-/-}$ lungs was the same as in WT and DKO lungs and cGMP levels in *Cav1*$^{-/-}$ lungs did not decrease compared with WT and DKO lungs. Importantly, treatment with either superoxide scavenger or NOS inhibitor reversed the PH of *Cav1*$^{-/-}$ mice, as did restoration of PKG activity through overexpression of PKG-1 in *Cav1*$^{-/-}$ lungs. In further support of the pathogenic role of PKG nitration, we identified the target tyrosine residues responsible for the impairment of PKG kinase activity following nitration. PKG-1α mutant with mutations at Tyr345 or Tyr549 located at the catalytic domain was resistant to peroxynitrite-induced tyrosine nitration and resultant impairment of PKG kinase activity. Both Tyr345 and Tyr549 are conserved from zebrafish to human PKG-1. Previous studies suggest that tyrosine nitration is enhanced by the close proximity of acidic residues (47–49). Consistent with these observations, the two target tyrosine residues are also next to an acidic residue.

NO-elicited *S*-nitrosylation has been demonstrated as an important mechanism regulating protein function (50). eNOS-mediated *S*-nitrosylation in mice that received a high dose of *N*-acetylcysteine was found to be involved in the pathogenesis of PH (51). However, our data demonstrated that there was no difference in total *S*-nitrosylation of proteins in *Cav1*$^{-/-}$ lungs compared with WT lungs, and the basal low levels of *S*-nitrosylation of PKG-1 in *Cav1*$^{-/-}$ lungs were similar to those in WT and DKO lungs. In addition, in vitro incubation with peroxynitrite but not DETA NONOate, a NO donor, resulted in impairment of PKG kinase activity. PKG kinase activity was in fact increased by DETA NONOate in intact vessels (52). High levels of NO itself (*Cav1*$^{-/-}$ mice treated with ROS scavenger) failed to promote the progression of PH but reversed PH in *Cav1*$^{-/-}$ mice. Taken together, these data strongly support the hypothesis that nitrative stress–induced PH in *Cav1*$^{-/-}$ mice is mediated by impaired PKG kinase activity through the tyrosine nitration.

Hypoxia has also been shown to impair PKG activity and PKG-mediated relaxation in ovine fetal intrapulmonary veins through both downregulation of PKG expression and tyrosine nitration of PKG (53), thus suggesting a role for PKG nitration in regulating hypoxic venoconstriction in utero. In contrast to our findings in *Cav1*$^{-/-}$ lungs, the hypoxia-induced tyrosine nitration of PKG in these studies was eNOS independent (53). Other studies showed that pulmonary vascular PKG expression was increased in chronically hypoxic rats, although the vasodilatory responses to exogenous NO and cGMP analog were attenuated (54). These data suggested that hypoxia-induced PKG nitration plays a role in the pathogenesis of hypoxia-induced PH. The present study provides direct mechanistic evidence of the critical role of the hypoxia-independent PKG nitration and resultant impairment of its kinase activity in mediating PH.

The balance between the protective and adverse effects of NO is determined by the relative amounts of NO and reactive oxygen species in the pathogenesis of PH (55). Here we show that PKG nitration resulting from eNOS activation secondary to caveolin-1 deficiency induces PH. Our data support the model outlined in Figure 9D according to which caveolin-1 deficiency results in persistent eNOS activation and hypoxia-independent production of reactive oxygen species and induces formation of peroxynitrite, which post-translationally modifies PKG through tyrosine nitra-

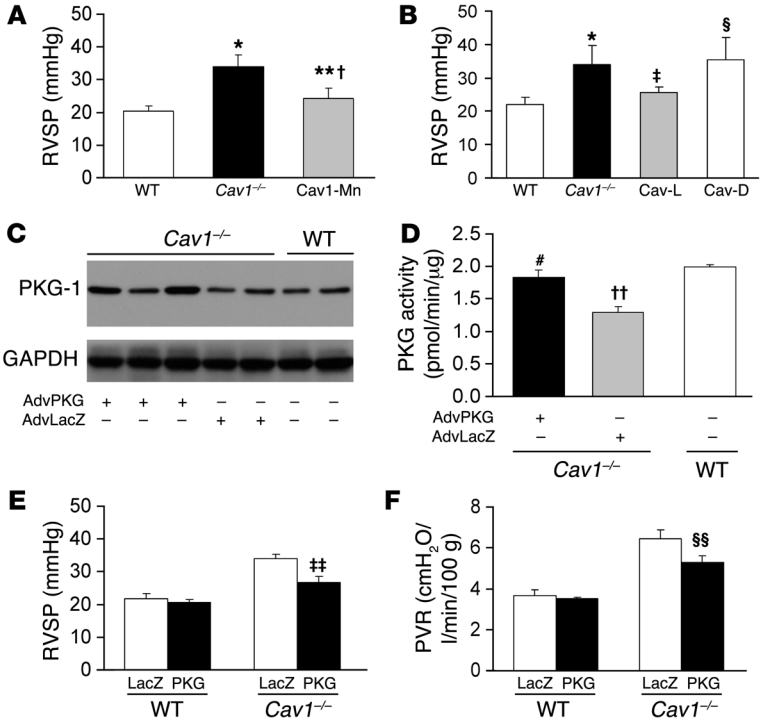

Figure 8
Tyrosine nitration–induced impairment of PKG activity mediates PH in *Cav1*$^{-/-}$ mice. (**A**) Reduced RVSP in *Cav1*$^{-/-}$ mice treated with MnTMPyP. *Cav1*$^{-/-}$ mice were treated with either MnTMPyP (5 mg/kg, i.p., daily) (Cav1-Mn) or saline (*Cav1*$^{-/-}$) for 6 weeks. Data are expressed as mean ± SD (n = 5 per group). *P < 0.01, *Cav1*$^{-/-}$ versus WT; **P < 0.05, Cav1-Mn versus *Cav1*$^{-/-}$; †P > 0.05, Cav1-Mn versus WT. (**B**) Inhibition of NOS with L-NAME reversed PH in *Cav1*$^{-/-}$ mice. *Cav1*$^{-/-}$ mice received water ad libitum (*Cav1*$^{-/-}$, control) or water with 1 mg/ml L-NAME (Cav-L) or its inactive analog D-NAME (Cav-D) for 5 weeks. Data are expressed as mean ± SD (n = 5–7). *P < 0.01, *Cav1*$^{-/-}$ versus WT; ‡P < 0.05, Cav-L versus *Cav1*$^{-/-}$; §P > 0.5, Cav-D versus *Cav1*$^{-/-}$. (**C**–**F**) Restoration of PKG-1 activity in *Cav1*$^{-/-}$ lungs reversed PH. At 7 days after administration of recombinant adenovirus expressing either human PKG-1 (AdvPKG) or LacZ, lungs were collected for Western blotting (**C**) and PKG kinase activity assay (**D**) after measurements of RVSP (**E**) and PVR (**F**). PKG activity is expressed as mean ± SD (n = 3–4). #P > 0.5 versus WT; ††P < 0.05 versus WT or *Cav1*$^{-/-}$ treated with AdvPKG (**D**). RVSP is expressed as mean ± SD (n = 4–5). ‡‡P < 0.05, *Cav1*$^{-/-}$-AdvPKG (PKG) versus *Cav1*$^{-/-}$-AdvLacZ (LacZ) (**E**). PVR is expressed as mean ± SD (n = 3–4). §§P < 0.05, *Cav1*$^{-/-}$-AdvPKG versus *Cav1*$^{-/-}$-AdvLacZ (**F**).

tion and impairs its kinase activity. Impaired PKG kinase activity in turn causes vasoconstriction and pulmonary vascular remodeling and thereby PH.

Previous studies showed a reduction in *CAV1* mRNA (56) and protein expression in lungs of patients with IPAH (23, 25). Decreased caveolin-1 expression in IPAH lungs was predominant in endothelial cells (25). Additionally, eNOS was robustly expressed in the plexiform lesions of IPAH lungs (57). To address the pathophysiological relevance of caveolin-1–regulated eNOS activity in the mechanism of increased PVR and vascular remodeling, we used lung tissue obtained from patients with IPAH. We observed decreased caveolin-1 expression and increased eNOS activity as well as increased PKG tyrosine nitration in IPAH lungs compared with normal lungs in the absence of marked changes in eNOS expression. These findings are in agreement with the studies in *Cav1*$^{-/-}$ mouse lungs described above.

In summary, we have demonstrated the crucial role of chronic activation of eNOS induced by loss of caveolin-1 in the pathogenesis of PH and provide evidence that hypoxia-independent PKG nitration induces PH. The results help to explain the mechanism of PH seen in patients with caveolin-1 deficiency (24, 25). Downregulation of caveolin-1 in lungs of IPAH patients occurred predominantly in endothelial cells (25), supporting the role of persistent eNOS activation induced by caveolin-1 deficiency in the mechanism of PH. Our results suggest the potential benefit of targeting increased eNOS activity and preventing nitration of PKG as novel therapy against IPAH.

Methods

Animals. To generate the DKO mice, we bred *Nos3*$^{-/-}$ mice into the background of *Cav1*$^{-/-}$ mice (The Jackson Laboratory). All mice were bred and maintained at the University of Illinois according to NIH guidelines. Approval for animal care and use for these experiments was granted by the Institutional Animal Care and Use Committee of the University of Illinois at Chicago.

Human subjects. Human lung tissues were obtained from patients undergoing lung transplantation for IPAH (n = 4; age 31.5 ± 19.2 years; 2 male, 2 female) and from unused donor lungs (n = 4; age 36.2 ± 16.1 years; all male). Informed consent from patients and local ethical approval from the Hammersmith Hospitals (ref. no. 2001/6003) and Royal Brompton & Harefield Hospitals (ref. no. 01-210) ethics committees were obtained prior to tissue collection.

Molecular analysis. Western blot analyses were performed using anti–caveolin-1 (1:1,000) and anti-iNOS (1:500; Santa Cruz Biotechnology Inc.), anti-eNOS (1:1,500) and anti-hsp90 (1:1,000; BD Biosciences), anti-nitrotyrosine (1:1,000, Millipore), anti-PKG-1 (1 μg/ml, a gift from X.-P. Du, Department of Pharmacology, University of Illinois at Chicago), anti-p42/44 and anti–phosphorylated p42/44 (1:1,000; Cell Signaling Technology), anti-VASP (1:1,000; Axxora), and anti–VASP phospho-Ser239 (1:200; Axxora). Anti–α-actin (1:4,000; Sigma-Aldrich) or anti-GAPDH (1:2,000; Santa Cruz Biotechnology Inc.) was used as a loading control. For detection of PKG-1 tyrosine nitration, protein lysates from either mouse or human lungs (500 μg each) or primary cultures of human pulmonary artery smooth muscle cells (80 μg each) were immunoprecipitated overnight with anti–PKG-1 (2 μg each) and then probed with anti-nitrotyrosine (1:2,500; Cayman Chemical).

RNA was isolated using an RNeasy Mini kit including DNase I digestion (QIAGEN), and quantitative RT-PCR analysis was performed in an ABI Prism 7000 Sequence Detection System (Applied Biosystems) with QuantiTect SYBR Green RT-PCR kit (QIAGEN). The sequences of the primers are provided in Supplemental Methods.

NO measurements. eNOS-derived NO from lung samples was measured by using the Griess Reagent System (Promega). Samples were incubated in 1 ml F-12 DMEM with inhibitors for iNOS (1,400W, 4 μM) and nNOS (N^{ω}-propyl-L-arginine, 1 μM) for 20 minutes. L-Arginine (1 mM) was then added and the samples incubated for 3 hours. Aliquots of medium were

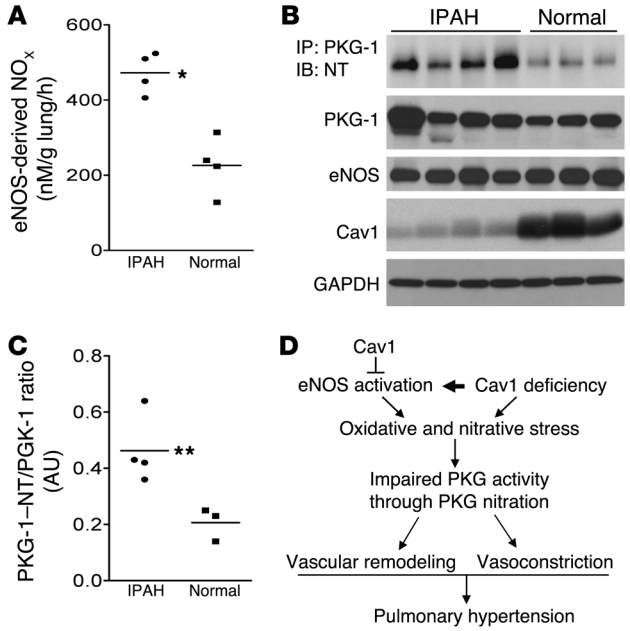

Figure 9

PKG tyrosine nitration in lung tissue from IPAH patients. (**A**) Quantitative analysis of eNOS-derived NO_x in human lung tissue. Following 20 minutes incubation with selective inhibitors, lung tissues were incubated with 1 mM L-arginine for 3 hours. eNOS-derived NO_x was determined by measuring the concentration of nitrite and nitrate in the medium with the Griess reagent. Bars represent mean. *$P < 0.01$ versus normal. IPAH lungs produced 2-fold greater eNOS-derived NO_x than normal lungs. (**B**) PKG tyrosine nitration in IPAH lungs. Each lysate (150 μg) was immunoprecipitated with anti–PKG-1 and immunoblotted with anti-nitrotyrosine for detection of PKG tyrosine nitration. IPAH lungs exhibited prominent PKG-1 tyrosine nitration compared with normal lungs. Protein levels of PKG-1, eNOS, and caveolin-1 were also determined by Western blotting with anti–PKG-1, -eNOS, or –caveolin-1 antibody, respectively. Immunoblot of GAPDH was used as loading control. (**C**) Densitometric analysis of PKG-1 tyrosine nitration. The intensity of each band of PKG-1 tyrosine nitration (PKG-1–NT) was normalized to the intensity of the respective PKG-1 band. PKG-1 tyrosine nitration increased 2-fold in IPAH lungs compared with normal lungs. Bars represent mean. *$P < 0.05$ (n = 3–4). (**D**) Proposed model of PKG nitration–mediated PH. Persistent eNOS activation secondary to caveolin-1 deficiency (*Cav1*$^{-/-}$ mice or IPAH patients) leads to formation of peroxynitrite in the pulmonary vasculature and impairment of PKG kinase activity through tyrosine nitration. Impaired PKG signaling induces pulmonary vascular remodeling and vasoconstriction, and thereby PH.

collected, and NO release was determined by measurement of the concentration of nitrite and nitrate (NO_x) in the aliquot in 2 steps using the Nitralyzer II kit (World Precision Instruments) and Griess reagent. Results are expressed as nanomolar/gram lung/hour incubation. Total NO_x production from mouse lung samples was determined with a similar method without incubation of NOS inhibitors. eNOS-derived NO from human lung samples was also determined using the 3-electrode system as detailed in Supplemental Methods.

Hemodynamic measurements. RVSP was determined with a 1.4F pressure transducer catheter (Millar Instruments) and AcqKnowledge software (Biopac Systems Inc.) as described previously (38). Briefly, the 1.4F pressure transducer was inserted through the right external jugular vein of anesthetized mice (100 mg ketamine/5 mg xylazine/kg BW, i.p.) and threaded into the right ventricle. RVSP was then recorded and analyzed with AcqKnowledge software.

PVR was measured as described previously (58). Briefly, the isolated lungs were ventilated (120/min and end expiratory pressure of 2.0 cmH_2O) and perfused at constant flow (2 ml/min) and venous pressure (+4 cmH_2O) with RPMI 1640 medium supplemented with 3 g/100 ml of BSA. Pulmonary arterial and venous pressure was monitored using pressure transducers (P23XL-1; Grass Technologies). PVR was calculated using the formula $(P_{pa} - P_{pv})/(Q/100\ g)$, where P_{pa} and P_{pv} are pulmonary arterial and venous pressure, and Q is flow (2 ml/min).

sGC enzyme activity and lung cGMP measurement. sGC enzyme activity and lung cGMP measurement are described in detail in Supplemental Methods.

PKG kinase assay. In vitro activity of PKG was determined by measuring the transfer of the [γ-^{32}P]phosphate group of ATP to the specific PKG substrate BPDEtide (Calbiochem) in the absence or presence of exogenous 2.5 μM cGMP as described previously (59) and in detail in Supplemental Methods. PKG activity is expressed as picomoles of ^{32}P incorporated into PKG substrate per minute per microgram protein.

Identification of nitrated tyrosine residues of PKG-1α. To determine the effects of nitration or nitrosylation on PKG activity, purified PKG-1 (Promega) was incubated with various concentrations of either peroxynitrite or DETA NONOate (Cayman Chemicals). Kinase activity was measured as described above. To identify the nitrated target tyrosine residues, tyrosine residue was mutated to phenylalanine by site-directed mutagenesis according to the manufacturer's instruction (Stratagene). Myc-tagged WT and mutant PKG-1α were overexpressed in human lung microvascular endothelial cells, and cell lysates were then immunoprecipitated with anti-Myc for 4 hours at room temperature. The same amount of immunoprecipitate was incubated with or without 100 μM peroxynitrite. After 14 minutes incubation in 50 mM K_2HPO_4 buffer at room temperature, kinase activity was then measured as described above.

Detection of protein S-nitrosylation. Detection of protein *S*-nitrosylation is described in detail in Supplemental Methods.

In vivo gene delivery to lungs. In vivo gene delivery to lungs is described in detail in Supplemental Methods.

Histology and imaging. Lung tissues were fixed and processed for H&E staining and immunofluorescence staining as described previously (60) and in detail in Supplemental Methods.

Statistics. Data are presented as mean ± SD. Statistical significance of differences between group means was determined using an unpaired 2-tailed Student's t test; a P value less than 0.05 was considered significant.

Acknowledgments

We thank X-P. Du of the University of Illinois and K.D. Bloch of Massachusetts General Hospital for their generosity in providing anti–PKG-1 antibody and recombinant AdvPKG, respectively; and R.A. Skidgel for critical comments concerning the manuscript. We also thank Jun Yuan, Liquan Cai, and Weijuan Yao for their expert technical support. This work was supported by NIH grants P01 HL060678 to A.B. Malik and R01 HL085462 to Y.-Y. Zhao.

Received for publication July 20, 2007, and accepted in revised form April 8, 2009.

Address correspondence to: You-Yang Zhao, Department of Pharmacology and Center for Lung and Vascular Biology, University of Illinois College of Medicine, 835 South Wolcott Avenue, Mail Code 868, Chicago, Illinois 60612, USA. Phone: (312) 355-0238; Fax: (312) 996-1225; E-mail: yyzhao@uic.edu.

1. Rubin, L.J. 1997. Primary pulmonary hypertension. *N. Engl. J. Med.* **336**:111–117.
2. Runo, J.R., and Loyd, J.E. 2003. Primary pulmonary hypertension. *Lancet.* **361**:1533–1544.
3. Rich, S. 2006. The current treatment of pulmonary arterial hypertension: time to redefine success. *Chest.* **130**:1198–1202.
4. Farber, H.W. 2008. The status of pulmonary arterial hypertension in 2008. *Circulation.* **117**:2966–2968.
5. Farber, H.W., and Loscalzo, J. 2004. Pulmonary arterial hypertension. *N. Engl. J. Med.* **351**:1655–1665.
6. Rabinovitch, M. 2008. Molecular pathogenesis of pulmonary arterial hypertension. *J. Clin. Invest.* **118**:2372–2379.
7. Lane, K.B., et al. 2000. Heterozygous germline mutations in BMPR2, encoding a TGF-beta receptor, cause familial primary pulmonary hypertension. The International PPH Consortium. *Nat. Genet.* **26**:81–84.
8. Machado, R.D., et al. 2006. Mutations of the TGF-beta type II receptor BMPR2 in pulmonary arterial hypertension. *Hum. Mutat.* **27**:121–132.
9. Humbert, M., et al. 2006. Pulmonary arterial hypertension in France: results from a national registry. *Am. J. Respir. Crit. Care Med.* **173**:1023–1030.
10. Hansmann, G., et al. 2008. An antiproliferative BMP-2/PPARγ/apoE axis in human and murine SMCs and its role in pulmonary hypertension. *J. Clin. Invest.* **118**:1846–1857.
11. Giaid, A., et al. 1993. Expression of endothelin-1 in the lungs of patients with pulmonary hypertension. *N. Engl. J. Med.* **328**:1732–1739.
12. Gross, S.S., and Wolin, M.S. 1995. Nitric oxide: pathophysiological mechanisms. *Annu. Rev. Physiol.* **57**:737–769.
13. Albrecht, E.W., Stegeman, C.A., Heeringa, P., Henning, R.H., and van Goor, H. 2003. Protective role of endothelial nitric oxide synthase. *J. Pathol.* **199**:8–17.
14. Miller, A.A., Hislop, A.A., Vallance, P.J., and Haworth, S.G. 2005. Deletion of the eNOS gene has a greater impact on the pulmonary circulation of male than female mice. *Am. J. Physiol. Lung Cell Mol. Physiol.* **289**:L299–L306.
15. Fulton, D., Gratton, J.P., and Sessa, W.C. 2001. Post-translational control of endothelial nitric oxide synthase: why isn't calcium/calmodulin enough? *J. Pharmacol. Exp. Ther.* **299**:818–824.
16. Bucci, M., et al. 2000. In vivo delivery of the caveolin-1 scaffolding domain inhibits nitric oxide synthesis and reduces inflammation. *Nat. Med.* **6**:1362–1367.
17. Michel, J.B., Feron, O., Sacks, D., and Michel, T. 1997. Reciprocal regulation of endothelial nitric-oxide synthase by Ca2+-calmodulin and caveolin. *J. Biol. Chem.* **272**:15583–15586.
18. Rothberg, K.G., et al. 1992. Caveolin, a protein component of caveolae membrane coats. *Cell.* **68**:673–682.
19. Drab, M., et al. 2001. Loss of caveolae, vascular dysfunction, and pulmonary defects in caveolin-1 gene-disrupted mice. *Science.* **293**:2449–2452.
20. Razani, B., et al. 2001. Caveolin-1 null mice are viable but show evidence of hyperproliferative and vascular abnormalities. *J. Biol. Chem.* **276**:38121–38138.
21. Zhao, Y.Y., et al. 2002. Defects in caveolin-1 cause dilated cardiomyopathy and pulmonary hypertension in knockout mice. *Proc. Natl. Acad. Sci. U. S. A.* **99**:11375–11380.
22. Mathew, R., et al. 2004. Disruption of endothelial-cell caveolin-1alpha/raft scaffolding during development of monocrotaline-induced pulmonary hypertension. *Circulation.* **110**:1499–1506.
23. Achcar, R.O., et al. 2006. Loss of caveolin and heme oxygenase expression in severe pulmonary hypertension. *Chest.* **129**:696–705.
24. Jasmin, J.F., Mercier, I., Dupuis, J., Tanowitz, H.B., and Lisanti, M.P. 2006. Short-term administration of a cell-permeable caveolin-1 peptide prevents the development of monocrotaline-induced pulmonary hypertension and right ventricular hypertrophy. *Circulation.* **114**:912–920.
25. Patel, H.H., et al. 2007. Mechanisms of cardiac protection from ischemia/ reperfusion injury: a role for caveolae and caveolin-1. *FASEB J.* **21**:1565–1574.
26. Beckman, J.S., and Koppenol, W.H. 1996. Nitric oxide, superoxide, and peroxynitrite: the good, the bad, and ugly. *Am. J. Physiol.* **271**:C1424–C1437.
27. Beckman, J.S., Beckman, T.W., Chen, J., Marshall, P.A., and Freeman, B.A. 1990. Apparent hydroxyl radical production by peroxynitrite: implications for endothelial injury from nitric oxide and superoxide. *Proc. Natl. Acad. Sci. U. S. A.* **87**:1620–1624.
28. Ferdinandy, P., Danial, H., Ambrus, I., Rothery, R.A., and Schulz, R. 2000. Peroxynitrite is a major contributor to cytokine-induced myocardial contractile failure. *Circ. Res.* **87**:241–247.
29. Feil, R., Lohmann, S.M., de Jonge, H., Walter, U., and Hofmann, F. 2003. Cyclic GMP-dependent protein kinases and the cardiovascular system: insights from genetically modified mice. *Circ. Res.* **93**:907–916.
30. Gow, A.J., et al. 2000. Two distinct mechanisms of nitric oxide-mediated neuronal cell death show thiol dependency. *Am. J. Physiol. Cell Physiol.* **278**:C1099–C1107.
31. Peng, Y.J., et al. 2006. Heterozygous HIF-1alpha deficiency impairs carotid body-mediated systemic responses and reactive oxygen species generation in mice exposed to intermittent hypoxia. *J. Physiol.* **577**:705–716.
32. Minshall, R.D., Sessa, W.C., Stan, R.V., Anderson, R.G., and Malik, A.B. 2003. Caveolin regulation of endothelial function. *Am. J. Physiol. Lung Cell Mol. Physiol.* **285**:L1179–L1183.
33. Gratton, J.P., et al. 2000. Reconstitution of an endothelial nitric-oxide synthase (eNOS), hsp90, and caveolin-1 complex in vitro. Evidence that hsp90 facilitates calmodulin stimulated displacement of eNOS from caveolin-1. *J. Biol. Chem.* **275**:22268–22272.
34. Pritchard, K.A., Jr., et al. 2001. Heat shock protein 90 mediates the balance of nitric oxide and superoxide anion from endothelial nitric-oxide synthase. *J. Biol. Chem.* **276**:17621–17624.
35. Murata, T., Sato, K., Hori, M., Ozaki, H., and Karaki, H. 2002. Decreased endothelial nitric-oxide synthase (eNOS) activity resulting from abnormal interaction between eNOS and its regulatory proteins in hypoxia-induced pulmonary hypertension. *J. Biol. Chem.* **277**:44085–44092.
36. Konduri, G.G., Ou, J., Shi, Y., and Pritchard, K.A., Jr. 2003. Decreased association of HSP90 impairs endothelial nitric oxide synthase in fetal lambs with persistent pulmonary hypertension. *Am. J. Physiol. Heart Circ. Physiol.* **285**:H204–H211.
37. Ozaki, M., et al. 2001. Reduced hypoxic pulmonary vascular remodeling by nitric oxide from the endothelium. *Hypertension.* **37**:322–327.
38. Zhao, Y.D., et al. 2005. Rescue of monocrotaline-induced pulmonary arterial hypertension using bone marrow-derived endothelial-like progenitor cells: efficacy of combined cell and eNOS gene therapy in established disease. *Circ. Res.* **96**:442–450.
39. Kim, Y.M., Bombeck, C.A., and Billiar, T.R. 1999. Nitric oxide as a bifunctional regulator of apoptosis. *Circ. Res.* **84**:253–256.
40. Wunderlich, C., et al. 2008. The adverse cardiopulmonary phenotype of caveolin-1 deficient mice is mediated by a dysfunctional endothelium. *J. Mol. Cell. Cardiol.* **44**:938–947.
41. Moens, A.L., and Kass, D.A. 2006. Tetrahydrobiopterin and cardiovascular disease. *Arterioscler. Thromb. Vasc. Biol.* **26**:2439–2444.
42. Mayer, B., et al. 1997. Tetrahydrobiopterin binding to macrophage inducible nitric oxide synthase: heme spin shift and dimer stabilization by the potent pterin antagonist 4-amino-tetrahydrobiopterin. *Biochemistry.* **36**:8422–8427.
43. Ozaki, M., et al. 2002. Overexpression of endothelial nitric oxide synthase accelerates atherosclerotic lesion formation in apoE-deficient mice. *J. Clin. Invest.* **110**:331–340.
44. Wunderlich, C., et al. 2008. Chronic NOS inhibition prevents adverse lung remodeling and pulmonary arterial hypertension in caveolin-1 knockout mice. *Pulm. Pharmacol. Ther.* **21**:507–515.
45. Murata, T., et al. 2007. Reexpression of caveolin-1 in endothelium rescues the vascular, cardiac, and pulmonary defects in global caveolin-1 knockout mice. *J. Exp. Med.* **204**:2373–2382.
46. Maniatis, N.A., et al. 2008. Increased pulmonary vascular resistance and defective pulmonary artery filling in caveolin-1–/– mice. *Am. J. Physiol. Lung Cell Mol. Physiol.* **294**:L865–L873.
47. Elfering, S.L., Haynes, V.L., Traaseth, N.J., Ettl, A., and Giulivi, C. 2004. Aspects, mechanism, and biological relevance of mitochondrial protein nitration sustained by mitochondrial nitric oxide synthase. *Am. J. Physiol. Heart Circ. Physiol.* **286**:H22–H29.
48. Ischiropoulos, H. 1998. Biological tyrosine nitration: a pathophysiological function of nitric oxide and reactive oxygen species. *Arch. Biochem. Biophys.* **356**:1–11.
49. Lanone, S., et al. 2002. Inducible nitric oxide synthase (NOS2) expressed in septic patients is nitrated on selected tyrosine residues: implications for enzymic activity. *Biochem. J.* **366**:399–404.
50. Hess, D.T., Matsumoto, A., Kim, S.O., Marshall, H.E., and Stamler, J.S. 2005. Protein S-nitrosylation: purview and parameters. *Nat. Rev. Mol. Cell Biol.* **6**:150–166.
51. Palmer, L.A., et al. 2007. S-nitrosothiols signal hypoxia-mimetic vascular pathology. *J. Clin. Invest.* **117**:2592–2601.
52. Qin, X., et al. 2007. cGMP-dependent protein kinase in regulation of basal tone and in nitroglycerin- and nitric oxide-induced relaxation in porcine coronary artery. *Pflugers Arch.* **454**:913–923.
53. Negash, S., et al. 2007. Regulation of cGMP-dependent protein kinase-mediated vasodilation by hypoxia-induced reactive species in ovine fetal pulmonary veins. *Am. J. Physiol. Lung Cell Mol. Physiol.* **293**:L1012–L1020.
54. Jernigan, N.L., Walker, B.R., and Resta, T.C. 2003. Pulmonary PKG-1 is upregulated following chronic hypoxia. *Am. J. Physiol. Lung Cell Mol. Physiol.* **285**:L634–L642.
55. Hampl, V., and Herget, J. 2000. Role of nitric oxide in the pathogenesis of chronic pulmonary hypertension. *Physiol. Rev.* **80**:1337–1372.
56. Geraci, M.W., et al. 2001. Gene expression patterns in the lungs of patients with primary pulmonary hypertension: a gene microarray analysis. *Circ. Res.* **88**:555–562.
57. Mason, N.A., et al. 1998. High expression of endothelial nitric oxide synthase in plexiform lesions of pulmonary hypertension. *J. Pathol.* **185**:313–318.
58. Parker, J.C., Gillespie, M.N., Taylor, A.E., and Martin, S.L. 1999. Capillary filtration coefficient, vascular resistance, and compliance in isolated mouse lungs. *J. Appl. Physiol.* **87**:1421–1427.
59. Gao, Y., et al. 2004. Role of cGMP-dependent protein kinase in development of tolerance to nitric oxide in pulmonary veins of newborn lambs. *Am. J. Physiol. Lung Cell Mol. Physiol.* **286**:L786–L792.
60. Zhao, Y.Y., et al. 2006. Endothelial cells-restricted disruption of FoxM1 impairs endothelial repair following LPS-induced vascular injury. *J. Clin. Invest.* **116**:2333–2343.